INORGANIC CHEMISTRY

FRONTIERS

Accepted Manuscript

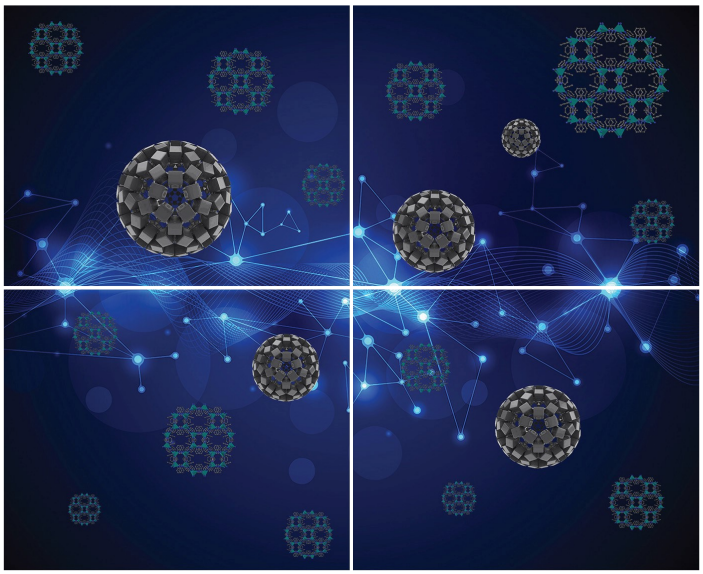

This article can be cited before page numbers have been issued, to do this please use: S. Liu, J. Han, R. Cui, X. Yang, Y. Fei, X. Tang, Y. Wang, Y. Wang, Y. Chen, J. Feng, H. Zheng, K. Li and X. Liu, *Inorg. Chem. Front.*, 2023, DOI: 10.1039/D3QI00829K.

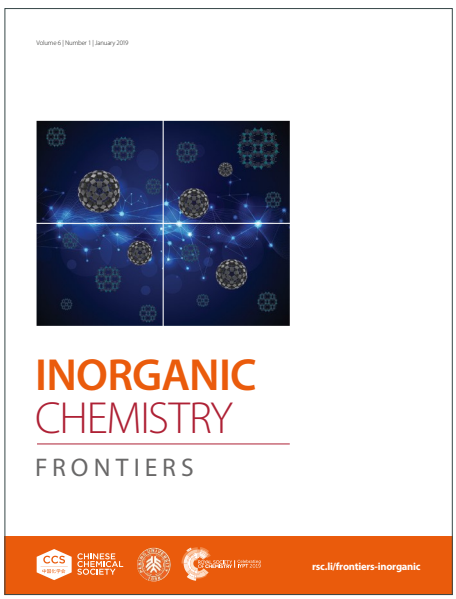

View Article Online
DOI: 10.1039/D3QI00829K

ARTICLE

Gd-doped diamond synthesized by Gd@C_{82} under high pressure and high temperature

Received 00th January 20xx,
Accepted 00th January 20xx

DOI: 10.1039/x0xx00000x

Shuhang Liu, ‡[a,b] Jun Han, ‡[b,d] Rongli Cui,[c] Xin Yang,[b] Yunfan Fei,[b] Xingyu Tang,[b] Yida Wang,[b] Yajie Wang,[b] Yongjin Chen,[b] Jiajia Feng,[b] Haiyan Zheng,[b] Kuo Li,*[b] Xiaoyang Liu*[a]

Diamond is an important industrial material with excellent physical properties. Transition-metal-doped diamond materials would have unexpected unique optical and magnetic properties, but they are difficult to synthesize. In this work, we synthesized Gd-doped diamond from endohedral metallofullerene (EMF) under high pressure and high temperatures up to 22 GPa and 2100 ℃. During room temperature compression up to 30 GPa, our Raman and IR results show that the carbon cage of Gd@C_{82} amorphized, while in situ X-ray diffraction (XRD) data still show clear 100 and 110 peaks, suggesting that the metal is still ordered. At 22 GPa and 2100 ℃, carbon transforms into diamond with larger lattice parameters as determined by XRD and High-Resolution Transmission microscopy (HRTEM). Gd distributes uniformly in the diamond matrix, which shows dilute paramagnetic properties and likely has charge transfer as indicated by Energy-dispersive spectra (EDS) mapping, Magnetic property measurement system (MPMS), and X-ray photoelectron spectroscopy (XPS). Our work synthesizes a rare-earth metal-doped diamond under high pressure and high temperature and sheds light on the synthesis of other metal-doped diamond materials.

Introduction

Doped diamond is a third-generation wide bandgap semiconductor material, with diverse electrical and magnetic properties depending on the different elements used for doping. Consequently, doped diamond has huge potential for various applications in electronic and electrochemistry devices, including electrodes, biosensors, and transistors.[1-5] Two common strategies for producing doped diamond are ion implantation and direct synthesis. Ion implantation is usually used to dope non-metallic elements into diamond.[6-9] Direct synthesis produces higher quality and more stable products than ion implantation, including high-pressure high-temperature synthesis and chemical vapor deposition.[10-13] Transition-metal-doped diamonds can only be prepared by direct synthesis. For example, Co and Ni-doped diamonds are synthesized in metal-carbon solvent catalysis systems.[14-16] The transition metal ion moves to the vacancy and sits at the center of the double semi-vacancy, forming a pseudo-octahedral environment. Density functional theory (DFT) calculations show that a Co-doped diamond is a ferromagnetically-ordered semiconductor with a small magnetic moment of 0.4 μB per supercell. Recently, a W-doped diamond has been reported and shows stable ferromagnetism, which originated from p-d hybridization between W-5d and C-2p state.[17] As shown in Fig. (1), we summarized different types of doped diamonds that have been reported to date[1-5,14-17]. However, until now, there has been no reported study of a rare-earth metal-doped diamond.

The main reason for this absence in the literature is that rare-earth metals are difficult to miscible with diamond. Therefore, we propose a bottom-up route to synthesize rare-earth-metal-doped diamond from endohedral metallofullerene (EMF) to overcome this.[18-21] Endohedral metallofullerenes form by encapsulating metal atoms, ions, or clusters inside carbon cages. In this work, we successfully doped representative rare-earth element Gd which has excellent magnetic properties and the largest spin quantum number into diamond using Gd@C_{82}'s unique metal-carbon cage structure as a precursor. We used both diamond anvil cell (DAC) and large-volume multi-anvil press (MAP),[22] achieving Gd-doped into diamond uniformly, which is beneficial for magnetic properties testing and structural analysis. It is efficient and unprecedented that synthesize rare-earth metal doped diamond by small molecule EMF under high pressure and high temperature. We first investigated the structure change of polycrystal Gd@C_{82} under high pressure with in situ X-ray diffraction (XRD), Raman, and Infrared spectra. The results show that Gd remains ordered in an amorphous carbon structure under high pressure. Then we synthesize Gd-doped diamond under high pressure and high temperature environment (HPHT) and confirmed it by XRD, high-angle annular dark-field scanning transmission electron

[a] State Key Laboratory of Inorganic Synthesis and Preparative Chemistry, College of Chemistry, Jilin University, Changchun 130012, China.
[b] Center for High Pressure Science and Technology Advanced Research (HPSTAR) , Beijing 100094, China.
[c] Institute of High Energy Physics, Chinese Academy of Sciences, 100049 Beijing, China.
[d] Department of Physics, Southern University of Science and Technology, Shenzhen 518055, China.
Electronic Supplementary Information (ESI) available: [details of any supplementary information available should be included here]. See DOI: 10.1039/x0xx00000x

View Article Online
DOI: 10.1039/D3QI00829K

ARTICLE

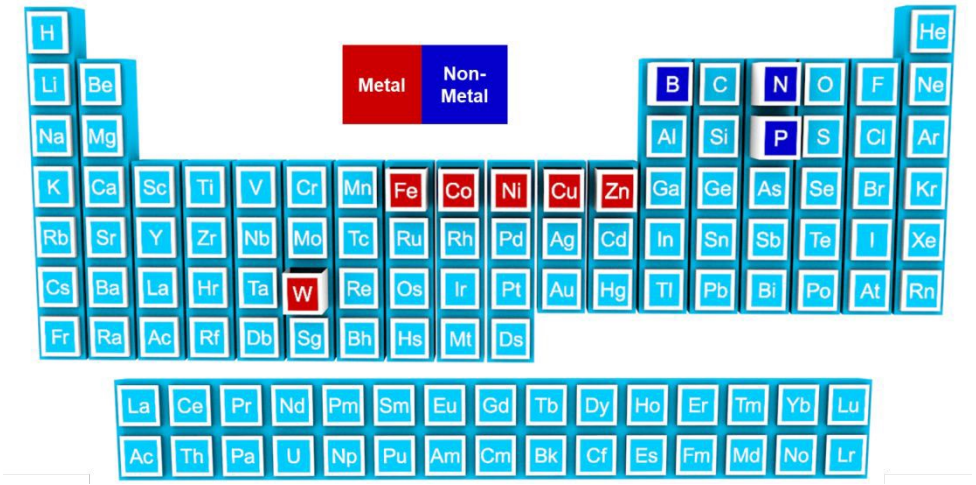

Figure 1. Reported doped diamond. Metal-doped diamond in red region, non-metal-doped diamond in blue region.[1-5,14-17]

microscopy (HAADF), Energy-dispersive spectra (EDS) and X-ray photoelectron spectroscopy (XPS). MPMS-3 (Quantum Design) measured the moment of the Gd-doped diamond, revealing its paramagnetic properties.

Experimental Methods

Sample preparation and Characterization

Gd@C_{82} polycrystals were synthesized by the continuous metallofullerene macro-scale preparation platform of the Institute of High Energy Physics, Chinese Academy of Sciences.[23-24] Amorphous Gd@C_{82} (99.157% in purity) was purchased from the Funano company. The purity was determined by high-performance liquid chromatography (HPLC). X-ray polycrystalline diffraction at atmospheric pressure was performed at the Pohang Accelerator Laboratory (PAL) synchrotron radiation station (λ = 0.69265 Å), as shown in Fig. S(1). A DAC equipped with diamonds with a culet size of 300 μm in diameter was used to generate high pressure. T-301 stainless steel gaskets were pre-compressed to about 35 μm in thickness, and a d = 120 μm hole was drilled as a sample chamber in the center of the gasket. Crystal samples were loaded into the sample chamber without a transmitting medium. A ruby ball was used to calibrate the pressure.[25]

The HP-HT experiment was performed using LP 1000-ton Walker equipment produced by the Max Voggenreiter company, the raw material was pressed into a pellet (1.3 mm in diameter and 1.4 mm in height) using hydrostatic pressing and then loaded into the Al_2O_3 capsules. The temperature range was 1800 ℃ -2100 ℃ , generated by a Re heater and the temperature was retained by $LaCrO_3$. The sample was assembled using tungsten carbide anvils with 3-mm, 5-mm truncation and 8-mm, 10-mm MgO octahedron. The temperature was monitored using a W5%Re-W26%Re type thermocouple, and the pressure was calibrated in the same way as reference.[26] The samples were compressed to 12, 14, 16, 20, and 22 GPa, respectively, with an 8/3 assembly and 15 GPa with a 10/5 assembly, then heated to the target temperature within 30 minutes. After quenching to room temperature and releasing pressure, the products were polished.

Measurement

The Raman experiment was performed on a Renishaw Micro-Raman spectroscopy system with a 488 nm Ar^+ laser, 532 nm second-harmonic Nd:YAG laser and 633 nm HeNe laser, respectively. The Raman spectra were recorded with a backscattering configuration, and we used a 1800 lines/mm and 2400 lines/mm grating, respectively. In situ infrared spectra were collected on a Bruker VERTEX 70v system with a HYPERION 2000 microscope. The spectra were collected in transmission mode with a range of 600-4000 cm^{-1} through an aperture of 20*20 μm^2. A resolution of 2 cm^{-1} was applied, and the absorption of the same diamond anvil region was used for the background to correct the data. The in situ XRD data was collected at the 5A XRS-MS beamline at Pohang Accelerator Laboratory (PAL). The wavelength of the X-ray beam was 0.69265 Å. A Mar345 detector calibrated by CeO_2 was used to collect the data. The XRD data of the MAP experiment products was collected at the beamline 4W2-high pressure experimental station at the Beijing Synchrotron Radiation Facility (BSRF). The X-ray wavelength was 0.6199 Å. A Pilatus 2M detector

View Article Online
DOI: 10.1039/D3QI00829K

calibrated by CeO_2 was used to collect data. The T-301 stainless steel plate that drilled 20 100μm diameter holes was used to load the samples. The XRD data for the sample synthesized at 20 GPa 1800 ℃ were collected on a PANalytical Empyrean (Cu Kα radiation; λ = 1.5418 Å). Dioptas and Jana 2006 software were used for integrating the data from the 2D XRD images and Lebail fitting of the powder XRD data, respectively.[27,28] The High-Resolution Transmission Electron Microscope (HRTEM) and Selected Area Electron Diffraction (SAED) patterns were recorded on a JEM-F200 (JEOL) with an accelerating voltage of 200 kV. The XPS spectra were tested by an American Thermo Fisher Scientific K-Alpha at the Huaxun company. The vacuum degree was 5×10^{-10} Pa, and the excitation source was Al Kα ray (hv = 1486.68 eV) with a working voltage of 15 kV. The signal accumulation of 5-10 cycles was carried out. The Passing-Energy was measured at 50 eV with a step size of 0.05 eV, and the charge correction was performed using the C_{1s} = 284.80 eV binding energy standard. The magnetization susceptibility was measured via Quantum Design MPMS-3 at 10 K which is calibrated by standard palladium reference sample after every cool down process. More details of characterization process are shown in Fig.S(2).

Results and discussion

In situ Raman spectra of Gd@C_{82} up to 13.8 GPa in the range of 100-2000 cm^{-1} are shown in Figs. 2(a) and (b), respectively. In order to avoid fluorescence interference, we used a laser with a wavelength of 633 nm to perform segmented data measurement in static mode. The Raman peaks in the range of 210-800 cm^{-1} are radial vibrations of the carbon cage. The peaks from 800-1050 cm^{-1} are the transition from the radial vibration of the carbon cage to the tangential vibration, and those at 1050-1700 cm^{-1} are the tangential stretching vibration of the carbon cage. The spectral peak at 1535 cm^{-1} (0.43 GPa) is attributed to the C=C stretching vibration, and the Raman peak blue shifts under high pressure due to the enhanced interatomic interactions[29-32]. Only the radial vibration of the carbon cage at 790 cm^{-1} Fig.S(3) redshifts due to the enhanced interaction between the carbon cages. Above 9.8 GPa, all the peaks began to disappear, indicating amorphization or polymerization. By maintaining the pressure at 13.8 GPa for one day and then releasing, no peak was observed during the decompression process, indicating that the carbon cage's destruction is irreversible.

Infrared absorption spectroscopy provides complementary information, which avoids the influence of fluorescence and provides more bonding information, as shown in Figs. 2(c) and (d). The radial vibration of the carbon cage at 795 cm^{-1} also redshifts with the increasing pressure, while the other spectral peaks blue shift. This is in consistence with Raman data, and indicates that Gd@C_{82} generally presents an enhanced interatomic force under high pressure. After 9.6 GPa, the spectral peaks began to

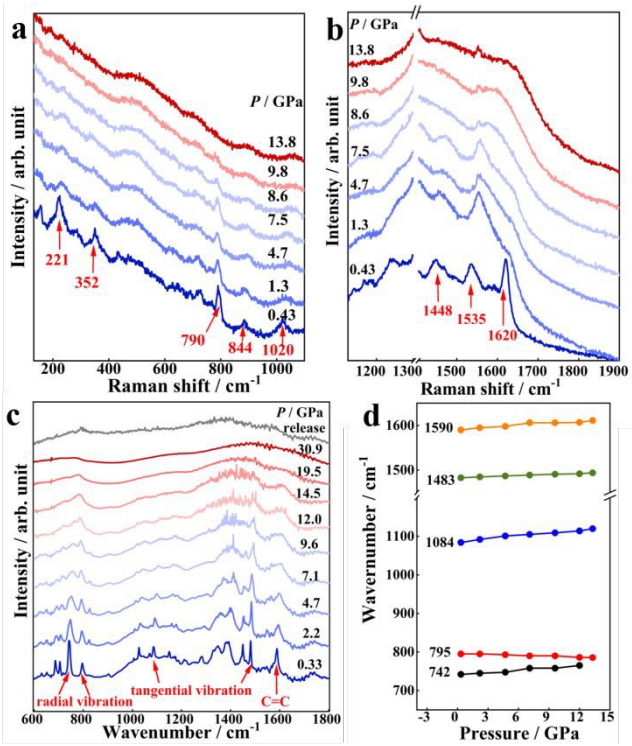

Figure 2. Selected Raman spectra of Gd@C_{82} upon compression. (a) In the range of 100-1100 cm^{-1}. (b) In the range of 1200-2000 cm^{-1}. (c) Selected Infrared absorption spectra of Gd@C_{82} upon compression and decompression. (d) Infrared peak position of Gd@C_{82} as a function of pressure.

disappear, indicating that the carbon cage began to be disintegrated. At 14.5 GPa, most of the spectral peaks had disappeared, indicating that the reaction could be completely amorphous or polymerized. The sample was preserved at 30.9 GPa for one day and then released. No obvious peak appeared, indicating that the carbon cage was broken and this process is irreversible.

To understand the change of Gd@C_{82} structure under high pressure, we investigated the in situ XRD of Gd@C_{82} up to 30.3 GPa, as shown in Fig. 3(a). A model structure of Gd@C_{82} based on the XRD results of 0 GPa was constructed and shown in Fig.S(1). At 0-13.9 GPa, all diffraction peaks move to a higher angle (high-Q), and the corresponding d-spacings become smaller, which indicates that Gd@C_{82} becomes denser with the increase in pressure. Above 13.9 GPa, the diffraction peak of 100 at 0.413 $Å^{-1}$ did not move, and the diffraction peak of 110 at 0.718 $Å^{-1}$ and 001 at 0.696 $Å^{-1}$ moved to the lower angle (low-Q, as shown in Fig. 3(b), which corresponds to the amorphous carbon cage observed in the Raman and IR spectra. The 100 and 110 peaks are maintained at 30 GPa, indicating that the Gd atoms may remain orderly after the destruction of the carbon cage. The sample was preserved at 30.8 GPa for six hours and

View Article Online
DOI: 10.1039/D3QI00829K

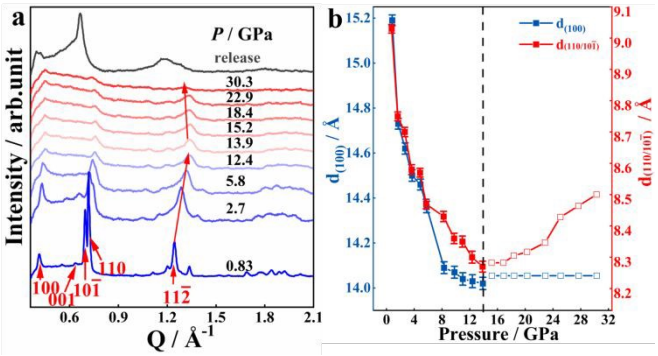

then released to ambient pressure. The peak of 100 and 110 still exist, which indicates the crystal still maintain partial order.

Figure 3. (a) Selected in-situ XRD patterns of polycrystal Gd@C_{82} upon compression and decompression. (b) D-spacing variation of the polycrystal under compression.

XRD results demonstrated that the Gd ion is still ordered at 30.9 GPa, which indicates that high pressure does not separate the Gd ion from the carbon phase. However, the carbon cage transforms into amorphous carbon. Then we added a temperature dimension using MAP equipment to obtain the Gd-diamond structure sample.[33-36] We selected six pressures to synthesize diamond at 1800 ℃ and implemented different temperature experiments three times at 22 GPa. Some doped diamond sample images are shown in Fig.S(4). The Raman spectra of the products show a peak at 1333 cm^{-1}, it can be seen in Fig.S(5) that is the first-order diamond Raman peak.[37] The broad peak between 1400-1550 cm^{-1} indicates the product contains residual C(sp^2) bonding.

We investigated XRD to obtain more structural information on the sample. Selected XRD patterns of the diamond samples are shown in Figs. 4(a) and (b). Our XRD results show that the cubic diamond phase was synthesized under HP-HT conditions. The diamond 111 peak at 3.05 $Å^{-1}$ is strong and sharp, which indicates excellent crystallinity. The corresponding lattice parameters were obtained by Le Bail fitting, as shown in Fig. 4(c). The result shows that the lattice parameters of diamond synthesized at 22 GPa are more enlarged above 0.02 Å than the reference.[38] We used pure carbon fullerene C_{60} as raw material to synthesized diamond at 22 GPa and 1800 ℃ as a control group to confirm that the lattice enlargement was not due to the change of synthesis conditions but to Gd doping into the diamond lattice.

The diffraction peak of the 22 GPa sample clearly broadened, which indicates the Gd-doped diamond crystallinity decreases. It may be caused by the higher density of the Gd doping into the diamond lattice defects at 22 GPa than in other synthesis conditions. According to the actual measurement of the peak full width at half maximum βs (FWHM), we calculated the grain size of the Gd-doped diamond using the Scherrer equation:[39]

$$Ls = \kappa\lambda/\beta s \cos(\theta^B)$$

where κ stands for a geometrical factor that fixes at 0.94. θ_B and λ represents the Bragg angle and wavelength (λ = 0.6199 Å). The grain size of the Gd-doped diamond synthesized at 22 GPa is about 10 nm, significantly decreased compared to the Gd-doped diamond synthesized under other conditions (~30 nm) and the control experiment (~20 nm). At 22 GPa, Gd doped into the diamond lattice more easily than in other conditions, thus reducing the diamond crystallinity and particle size.

The microscopic features of the Gd-doped diamond were

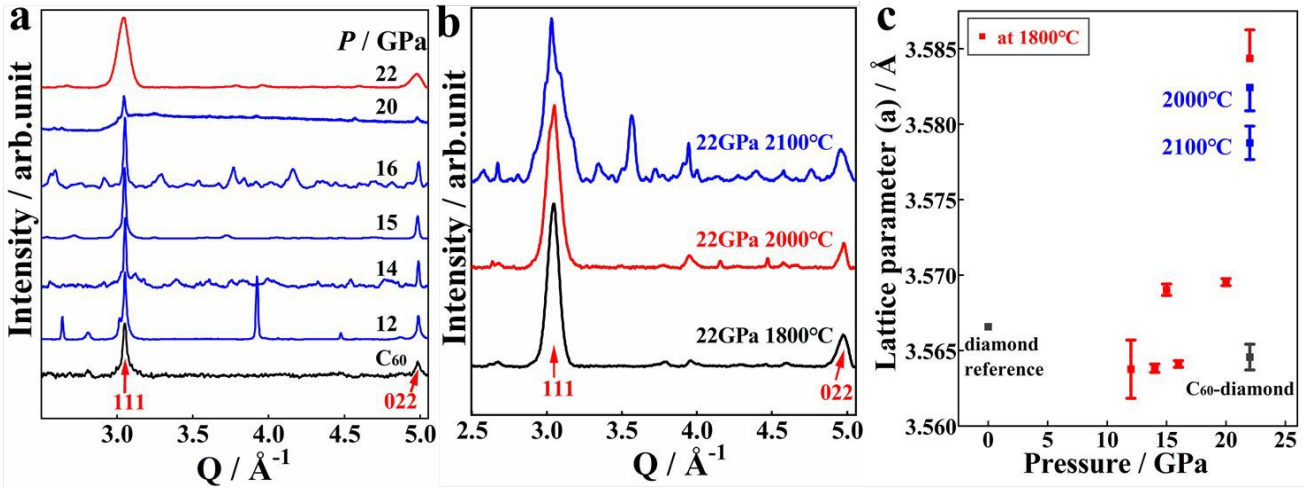

Figure 4. XRD patterns and lattice parameters with Le Bail fitting. (a) XRD of diamond synthesized by C_{60} and Gd@C_{82} at 1800 ℃ with different temperatures (b) XRD of GdC_{82} diamond synthesized under 22 GPa with different temperatures. (c) lattice parameter changes with the error bar of Gd-doped diamond and standard diamond lattice parameter for reference.

View Article Online
DOI: 10.1039/D3QI00829K

ARTICLE

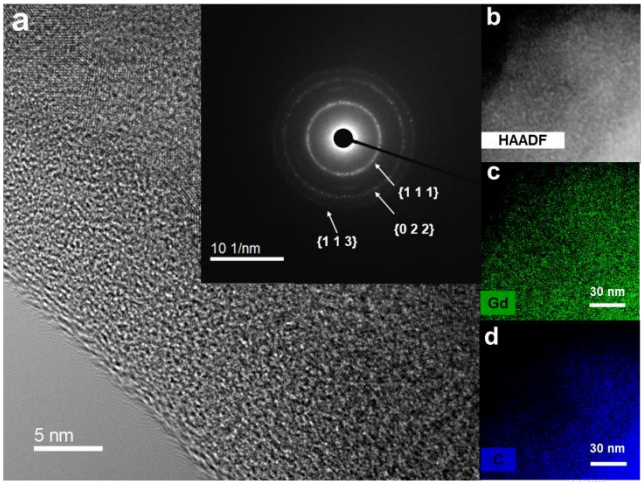

Figure 5. (a) HRTEM and selected area electron diffraction (SAED) images of the Gd-doped diamond recovered from 22 GPa and 1800 ℃. (b) HAADF-STEM image of the 22 GPa and 1800 ℃ sample. EDS mapping of the (c) Gadolinium overlay and (d) carbon overlay.

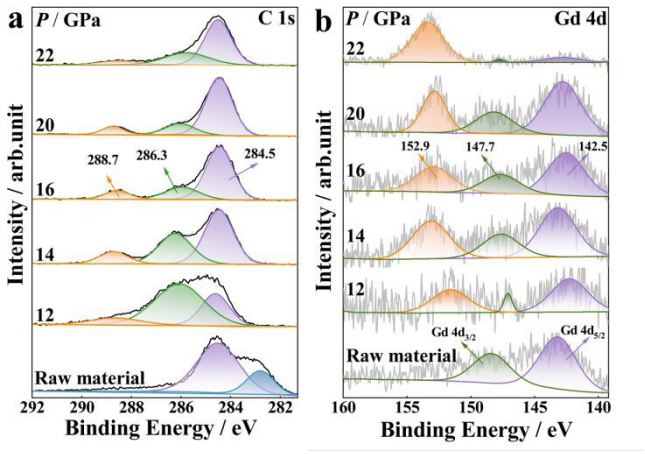

Figure 6. XPS spectra of the raw material Gd@C_{82} and Gd-doped diamond synthesized from 12 GPa to 22 GPa and 1800 ℃: (a) C_{1s} region, (b) Gd_{4d} region.

scrutinized with High-Resolution Transmission microscopy (HRTEM). The HRTEM images of the 22 GPa 1800 ℃ sample are shown in Fig. 5(a). The HRTEM images of 15 GPa and 1800 ℃ sample are shown in Fig. S(6). Obvious lattice fringes are found in the 15 GPa and 1800 ℃ sample, and the diffraction rings are bright and clear. The pattern of the 22 GPa and 1800 ℃ sample shows that the diffraction ring's intensity weakened and the HRTEM image finds a more random arrangement than the sample under 15 GPa and 1800 ℃.

Nanoscale elemental compositional analysis was carried out by energy-dispersive spectroscopy (EDS) mapping in TEM with high spatial resolution. High-angel annular dark-field (HAADF) STEM image of 22 GPa 1800 ℃ sample are shown in Fig. 5(b). The elemental distribution of Gd and C in the doped diamond sample is shown in Fig. 5(c)(d). Gd and C elements diffuse uniformly and no obvious enriched Gd phase appears. We measured the EDS mapping of the Gd@C_{82} raw material for comparison as shown in Fig. S(7), which shows that the Gd element is uniformly dispersed in the region of the carbon element. When the carbon cage of Gd@C_{82} transforms into the diamond under HPHT conditions, no Gd-containing phase appears. The Gd elements are still uniformly distributed in the carbon region and are retained in the diamond lattice.

To investigate the local Gd-C interaction, XPS experiment was performed for the raw material Gd@C_{82} and the Gd-doped diamond samples as shown in Fig. (6). Comparing the Gd4d core-level spectra as shown in Fig. 6(a) with the XPS references shows that the Gd4d core-level spectra have peaks of Gd@C_{82} at 143.2 eV and 148.3 eV represented the Gd $4d_{5/2}$ and Gd $4d_{3/2}$ respectively.[40] Compared with the raw material, the binding energy of the Gd_{4d} core level in doped diamond decreased, indicating that the valence shell of Gd ions changed. The greatest difference between the doped diamond and the raw materials XPS data is the new peak of the high-intensity XPS band located at 152.9 eV, which is likely related to the charge transfer process during Gd-doped diamond formation. The same phenomenon also occurs in the Gd-SiO_2 system,[41] where it is contributed by the Gd-C bonding formation. We can also see the corresponding transformation in the XPS C_{1s} spectra. Fig. 6(b) shows the core level XPS C_{1s} spectra of the Gd@C_{82} raw material and Gd-doped diamond. For the raw material, the two fitting peaks originate from the contribution of carbon in the carbon cage of EMF with different chemical environments.[42] According to the existing reports, carbon atoms with the sp^3 state line are in the range of 284.1-285.2 eV, and few appear at the values of 286.0 eV.[43,44] The binding energy of 286.3 and 284.5 eV in the doped diamond XPS spectra was consistent with the binding energy of nanodiamond. The peak of 288.7 eV is not attributed to the pure carbon nanodiamond. We determined that a small portion of the carbon in the nanodiamond interacts with Gd, which produces a binding energy increase to 288.7 eV. This fact shows that Gd doped into the diamond lattice during formation.

The magnetic properties of Gd-doped diamond were characterized by MPMS-3 (Quantum Design). The inverse of the magnetic moment as a function of the temperature between 2 K and 300 K at constant field H = 50 Oe after zero-field cooling (ZFC) or field cooling (FC) of the Gd-doped diamond sample synthesized at 22 GPa and 2000 ℃ are shown in Fig. 7(a). The sample exhibits obvious paramagnetic properties in the temperature region above 200 K. We

View Article Online
DOI: 10.1039/D3QI00829K

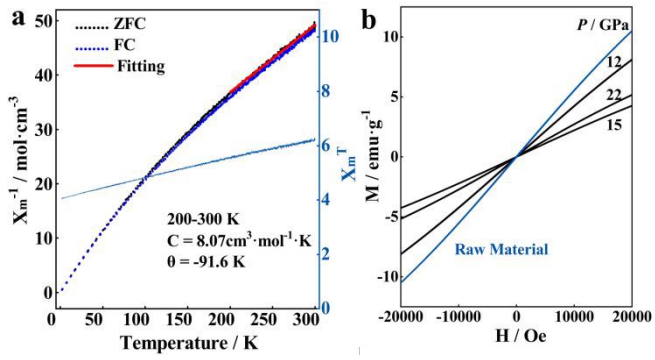

Figure 7. (a) Inverse of the magnetic moment as a function of the temperature between 2 K and 300 K measured at a constant magnetic field H=50 Oe after ZFC or FC curve. (b) Magnetization at 10 K of raw material Gd@C_{82} and Gd-doped diamond synthesized from 12 GPa and 1800 ℃, 15 GPa and 1800 ℃, and 22 GPa and 2000 ℃.

fitted magnetic susceptibility of Gd-doped diamond by Curie-Weiss law:[45]

$$\chi^m = C/(T - T^C)$$

Where C stands for Curie constant. Tc represents the Curie temperature. The fitting result shows a Curie constant of C=8.07cm³·mol⁻¹·K and a Weiss constant of θ = -91.6 K. Calculated from $8C = \mu_{eff}^2/\mu_B^2$, effective magnetic moment μ_{eff} = 8.07μ_B. This is the typical effective magnetic moment value of the Gd^{3+}. The magnetization curves of the Gd-doped diamonds are shown in Fig. 7(b). The results indicate that Gd-doped diamonds retain their paramagnetic characteristics from the raw material. The M-T curve of raw material was shown in Fig. S(8). Intrinsic diamond possesses diamagnetic characteristics, while the Gd-doped diamond shows paramagnetic characteristics at 10 K, indicating that the process of transformation to diamond retains paramagnetic characteristics of Gd element.

Conclusions

In summary, we synthesized Gd-doped diamond via the polymerization of Gd@C_{82}. The polymerization of Gd@C_{82} starts at about 13 GPa. With further increasing pressure, the products start disordering. We obtained Gd-doped diamond from 12-22 GPa and 1800-2100 ℃, with the grain size of 10s of nanometer. The volume of the diamond crystal enlarged by about 2% caused by the Gd doped in the diamond crystal cell. Furthermore, the EDS mapping shows the uniform elemental distribution of gadolinium and carbon. The new peaks in the XPS Gd_{4d} and C_{1s} spectra originate from charge transfer between Gd and C in the Gd-doped diamond. The magnetization curves indicate that the Gd-doped diamond exhibits paramagnetic properties and could have great potential for applications in micro-electro-mechanical systems. Synthesis rare-earth metal doped diamond by small molecule EMF Gd@C_{82} achieves effective Gd doping, which indicates EMF can be an excellent precursor for synthesizing various of doped diamond and broadens the application of doped diamond in the future.

Author contributions

Shuhang Liu and Jun Han did the experiments, analyzed the data, wrote the paper and should be considered co-first authors. Kuo Li, Haiyan Zheng and Xiaoyang Liu designed the research, Shuhang Liu synthesized the sample, RongLi Cui, Xin Yang, Yunfan Fei, Yajie Wang, Yongjin Chen and Jiajia Feng provide equipment. Xin Yang, Yida Wang and Xingyu Tang help analyse data with software. All authors have approved the final version of the manuscript.

Conflicts of interest

There are no conflicts to declare.

Acknowledgements

This research was supported by the National Natural Science Foundation of China (NSFC) (Nos. 22171101, 22022101, 21771011). We thank Dr. Hyun Hwi Lee for supporting the in situ XRD measurements under high pressure.

Notes and references

1 S. Talapatra, P. G. Ganesan, T. Kim, R. Vajtai, M. Huang, M. Shima, G. Ramanath, D. Srivastava, S.C. Deevi, and P. M. Ajayan, Irradiation-induced magnetism in carbon nanostructures, *Phys. Rev. Lett*., 2005, **95**, 097201.

2 A. E. Rugar, H. Lu, C. Dory, S. Sun, P. J. McQuade, Z. Shen, N. A. Melosh, and J. Vučković, Generation of Tin-Vacancy centers in diamond shallow ion implantation and subsequent diamond overgrowth, *Nano Lett*., 2020, **20**, 1614-1619.

3 R. Höhne, P. Esquinazi, V. Heera, and H. Weishart, Magnetic properties of ion-implanted diamond, *Diam Relat. Mater*., 2007, **16**, 1589-1596.

4 C. A. Salamanca-Neto, F. Yoshida, E. R. Sartori, and J. T. Moraes, Boron-doped diamond electrode: a modification-free platform for sensitive square-wave voltammetric determination of indapamide hydrochloride, *Anal. Methods.,* 2018, **10**, 3347-3352.

5 M. Yence, A. Cetinkaya, G. Ozcelikay, S. I. Kaya, and S. A. Ozkan, Boron-doped diamond electrodes: recent decelopments and advances in view of electrochemical drug sensors, *Crit Rev Anal Chem*., 2022, **52**, 1122-1138.

6 N. Chen, H. A. Ma, B. Yan, L. Chen, L. Chen, L. Guo, X. Miao, C. Fang, and X. Jia, Characaterization of various centers in synthetic type Ib diamond under HPHT annealing, *Cryst. Growth Des.,* 2018, **18**, 3870-3876.

View Article Online
DOI: 10.1039/D3QI00829K

7 M. J. Crane, A. Petrone, R. A. Beck, M. B. Lim, X. Zhou, X. Li, R. M. Stroud, and P. J. Pauzauskie, High-pressure, high-temperature molecular doping of nanodiamond, *Sci. Adv.,* 2019, **5**, eaau6073.

8 E. A. Ekimov, O. S. Kudryavtsev, S. Turner, S. Korneychuk, V. P. Sirotinkin, T. A. Dolenko, A. M. Vervald, and I. I. Vlasov, The effect of molecular structure of organic compound on the direct high-pressure synthesis of boron-doped nanodiamond, *Phys. Status Solidi.,* 2016, **213**, 1-8.

9 A. Sherehiy, S. Dumpala, M. K. Sunkara, J. B. Jasinski, R. W. Cohn and G. U. Sumanasekera, Thermionic emission from phosphorus (P) doped diamond nanocrystals supported by conical carbon nanotubes and Ultraviolet Photoelectron spectroscopy study of P-doped diamond films, *Diam Relat. Mater*., 2014, **50**, 66-76.

10 M. D. Feudis, A. Tallaire, L. Nicolas, O. Brinza, P. Goldner, G. Hétet, F. Bénédic, and J. Achard, Large-Scale fabrication of highly emissive nanodiamonds by chemical vapor deposition with controlled doping by SiV and Gev centers from a solid source, *Adv. Mater. Interfaces.,* 2020, **7**, 1901408.

11 A. T. Colliins, A. Connor, C. Ly, A. Shareef, and P. M. Spear, High-temperature annealing of optical centers in typer-I diamond, *J. Appl. Phys.,* 2005, **97**, 083517.

12 Q. Liang, C. Yan, Y. Meng, J. Lai, S. Krasnicki, H. Mao, and R. J. Hemley, Recent advances in high growth rate single-crystal CVD diamond, *Diam Relat. Mater*., 2009, **18**, 698-703.

13 M. J. Crane, B. E. Smith, P. B. Meisenheimer, X. Zhou, R. M. Stroud, E. J. Davis, and P. J. Pauzauskie, Photothermal effects during nanodiamond synthesis from a carbon aerogel in a laser-heated diamond anvil cell, *Diam Relat. Mater*., 2018, **87**, 134-142.

14 E. B. Lombardi, Co in diamond: Ferromagnetic ordering of a transition metal in diamond, *Diam Relat. Mater*., 2008, **17**, 1345-1348.

15 E. Gheetaert, A. Kumar, E. Bustarret, L. Ranno, L. Magaud, and Y. Joly, Investigation of nickel lattice sites in diamond: Density functional theory and x-ray absorption near-edge structure experiments, *Phys. Rev. B.,* 2012, **86**, 054116.

16 E. M. Benecha, E. B. Lombardi, Cu doped diamond: Effect of charge state and defect aggregation on spin interactions in a *3d* transition metal doped wide band-gap semiconductor, *J. Appl. Phys*., 2018, **123**, 185706.

17 J. Su, R. Wang, H. Wang, and H. Fan, Investigation on magnetic properties of W-doped diamond via first-principles, *Diam Relat. Mater*., 2022, **129**, 109306.

18 X. Lu, T. Akasaka, and S. Nagase, Chemistry of Endohedral Metallofullerenes: The Role of Metals, *Chem. Commun.,* 2011, **47**, 5942-5957.

19 A. A. Popov, S. Yang, and L. Dunsch, Endohedral fullerenes, Chem. Rev., 2013, **113**, 5989-6113.

20 B. Sundqvist, Carbon under pressure, *Phys. Rep.,* 2021, **909**, 1-73.

21 N. Dubrovinskaia, L. Dubrovinsky, F. Langenhorst, S. Jacobsen, and C. Liebske, Nanocrystalline diamond synthesized from C_{60}, *Diam Relat. Mater*., 2005, **14**, 16-22.

22 Y. Shang, Z. Liu, J. Dong, M. Yao, Z. Yang, Q. Li, C. Zhai, F. Shen, X. Hou, L. Wang, N. Zhang, W. Zhang, R. Fu, J. Ji, X. Zhang, H. Lin, Y. Fei, B. Sundqvist, W. Wang, and B. Liu, Ultrahard bulk amorphous carbon from collapsed fullerene, *Nature.,* 2021, **599**, 599-604.

23 B. Sun, T. Sugai, E. Nishibori, K. Iwata, M. Skata, M. Takata, and H. Shinohara, An anomalous endohedral structure of Eu@C_{82} metallofullerenes, *Angew. Chem. Int. Ed.,* 2005, **44**: 4568-4571.

24 B. Sun, L. Feng, Z. Shi, and Z. Gu, Improved extraction of metallofullerenes with DMF at high temperature, *Carbon.,* 2002, **40**: 1591-1595.

25 H. Mao, J. Xu, and P. M. Bell, Calibration of Ruby pressure Gauge to 800 kbar under Quasi-hydrostatic conditions, *J. Geophys. Res*., 1986, **91**, 4673-4676.

26 Y. C. Shang, F. R. Shen, X. Y. Hou, L. Y. Chen, K. Hu, X. Li, R. Liu, Q. Tao, and P. Zhu, Pressure generation above 35GPa in a Walker-Type Large-Volume Press. *Chin. Phys. Lett.,* 2020, **37**, 080701.

27 C. Prescher, and V. B. Prakapenka, DIOPTAS: a Program for Reduction of Two-dimensional X-ray Diffraction Data and Data Exploration, *High Press Res.,* 2015, **35**, 223-230.

28 V. Petříček, M. Dušek, and L. Palatinus, Crystallographic computing system JANA2006: general features, *Z. Krist-Cryst Mater*., 2014, **229**: 345-352.

29 V. V. Zhukov, S. V. Erohin, V. D. Churkin, N. G. Vnukova, L. Yu. Antipina, V. I. Elesina, M. A. Visotin, Ye. V. Tomashevich, M. Yu. Popov, G. N. Churilov, P. B. Sorokin, and A. S. Fedorov, Feature of the Endohedral Metallofullerene Y@C_{82} and Gd@C_{82} Polymerization under high pressure, *J. Phys. Chem. C.,* 2022, **126**, 17366-17373.

30 S. V. Erohin, V. D. Churkin, N. G. Vnukova, M. A. Visotin, E. A. Kovaleva, V. V. Zhukov, L. Yu. Antipina, Ye. V. Tomashevich, Yu. L. Mikhlin, M. Yu. Popov, G. N. Churilov, P. B. Sorokin and A. S. Fedorov, Insights into fullerene polymerization under the high pressure: The role of endohedral Sc dimer, *Carbon.,* 2022, **189**, 37-45.

31 M. Krause, P. Kuran, U. Kirbach, and L. Dunsch, Raman and infrared spectra of Tm@C_{82} and Gd@C_{82}, *Carbon* 1999, **37**, 113-115.

32 R. Nishibori, M. Takata, M. Sakata, H. Tanaka, M. Hasegawa, and H. Shinohara, Giant motion of La atom inside C_{82} cage, *Chem. Phys. Lett.,* 2000, **330**, 497-502.

33 Z. Zeng, J. Wen, H. Lou, X. Zhang, L. Yang, L. Tan, B. Cheng, X. Zuo, W. Yang, W. L. Mao, H. Mao, and Q. Zeng, Preservation of high-pressure volatiles in nanostructured diamond capsules, *Nature.,* 2022, **608**, 513-517.

34 Z. Zeng, L. Yang, Q. Zeng, H. Lou, H. Sheng, J. Wen, D. J. Miller, Y. Meng, W. Yang, W. L. Mao, and H, Mao, Synthesis of quenchable amorphous diamond, *Nat. Commun.,* 2017, 8, 322.

35 H. Tang, X. Yuan, Y. Cheng, H. Fei, F. Liu, T. Liang, Z. Zeng, T. Ishii, M. Wang, T. Katsura, H. Sheng, and H. Gou, Synthesis of Paracrystalline Diamond, *Nature.,* 2021, **599**, 605-610.

36 K. Luo, B. Liu, W. Hu, X. Dong, Y. Wang, Q. Huang, Y. Gao, L. Sun, Z. Zhao, Y. Wu, Y. Zhang, M. Ma, X. Zhou, J. He, D. Yu, Z. Liu, B. Xu, and Y. Tian, Coherent interfaces govern direct transformation from graphite to diamond, *Nature*., 2022, **607**,486-491.

37 H. Herchen, and M. A. Cappelli, First-order Raman spectrum of diamond at high temperatures, *Phys. Rev. B.*, 1991, **43**, 11740.

38 H. J. Grenville-Wells, and K. Lonsdale, X-ray study of laboratory-made diamonds, *Nature.,* 1958, **181**, 758-759.

39 A. L. Patterson, The Scherrer formula for X-ray particle size determination, *Phys. Rev*., 1939, **56**, 978.

40 B. Vincent-Crist, Handbook of monochromatic XPS spectra: The elements of native oxides. John Wiley & Sons, 2000.

41 A. F. Zatsepin, D. A. Zatsepin, D. W. Boukhvalov, Yu. A. Kuznetsova, N. V. Gavrilov, V. Ya. Shur, and A. A. Esin, Local

View Article Online
DOI: 10.1039/D3QI00829K

atomic configurations, energy structure, and optical properties of implantation defects in Gd-doped silica glass: an XPS, PL, and DFT study, *J. Alloys Compd.,* 2019, **796**, 77-85.

42 J. Kim, Y. Yamada, M. Kawai, T. Tanabe, and S. Sato, Spectral change of simulated X-ray photoelectron spectroscopy from graphene to fullerene. *J. Mater. Sci.,* 2015, **50**, 6739-6747.

43 M. Yeganeh, P. R. Coxon, A. C. Brieva, V. R. Dhanak, L. Šiller, and Yu. V. Butenko, Atomic hydrogen treatment of nanodiamond powder studied with photoemission spectroscopy. *Phys. Rev. B.,* 2007, **75**, 155404.

44 A. T. Kozakov, A. G. Kochur, N. Kumar, K. Panda, A. V. Nikolskii, and A. V. Sidashov, Determination of sp2 and sp3 phase fractions on the surface of diamond films from C1s, valance band X-ray photoelectron spectra and CKVV X-ray-excited Auger spectra. Appl. Surf. Sci., 2021, **536**, 147807.

45 H. Yao, X. Ning, H. Zhao, A. Hao, and M. Ismail, Effect of Gd-Doping on Structural, Optical, and Magnetic Properties of $NiFe_2O_4$ As-prepared Thin Films via Facile Sol-Gel Approach. *ACS Omega* 2021, **6**, 6305-6311.